BIOLOGY OF REPRODUCTION **65,** 680–688 (2001)

# Cellular Turnover in the Mammary Gland Is Correlated with Systemic Levels of Progesterone and Not 17β-Estradiol During the Estrous Cycle[1]

**Jimmie E. Fata, Varun Chaudhary, and Rama Khokha[2]**

*Department of Medical Biophysics and Department of Laboratory Medicine and Pathobiology, Ontario Cancer Institute, University of Toronto, Toronto, Ontario, Canada M5G 2M9*

## ABSTRACT

**Adult mammary tissue has been considered "resting" with minimal morphological change. Here, we reveal the dynamic nature of the nulliparous murine mammary gland. We demonstrate specific changes at the morphological and cellular levels, and uncover their relationship with the murine estrous cycle and physiological levels of steroid hormones. Differences in the numbers of higher-order epithelial branches and alveolar development led to extensive mouse-to-mouse mammary variations. Morphology (assigned grades 0–3) ranged from a complete lack of alveoli to the presence of numerous alveoli emanating from branches. Morphological changes were driven by epithelial proliferation and apoptosis, which differed between ductal versus alveolar structures. Proliferation within alveolar epithelium increased as morphological grade increased. Extensive alveolar apoptosis was restricted to tissue exhibiting grade 3 morphology, and was ~14-fold higher than at all other grades. Epithelial proliferation and apoptosis exhibited a positive relationship with serum levels of progesterone, but not with 17β-estradiol. Compared with other estrous stages, diestrus was unique in that the morphological grade, epithelial proliferation, apoptosis, and progesterone levels all peaked at this stage. The regulated tissue remodeling of the mammary gland was orchestrated with mRNA changes in specific matrix metalloproteinases (MMP-9 and MMP-13) and specific tissue inhibitors of metalloproteinases (TIMP-3 and TIMP-4). We propose that the cyclical turnover of epithelial cells within the adult mammary tissue is a sum of spatial and functional coordination of hormonal and matrix regulatory factors.**

*apoptosis, estradiol, mammary glands, ovulatory cycle, progesterone*

## INTRODUCTION

The mouse mammary gland provides researchers with a tool for examining many aspects of developmental, endocrine, and tumor biology. With the development of transgenic and knockout technology in the last two decades, this organ has seen a large increase in its laboratory use. Within the last 2 yr numerous publications have examined mammary gland biology in transgenic or knockout mice, and many more have used genetically unmanipulated tissue. However, to date no studies have investigated the natural variations in mouse mammary gland morphology, proliferation, apoptosis, and their relationship to the normal hormonal fluctuation of the estrous cycle. There is a need to establish the normal range of physiological changes in the mammary gland of nulliparous adult mice to facilitate accurate interpretations of mammary gland phenotypes. A full elucidation of the extent of these physiological changes is fundamental to our understanding of this tissue.

A mammary gland isolated from an adult nulliparous female mouse undergoes multistaged parenchymal development and differentiation [1, 2]. These stages can be classified as fetal, prepubescence, pubescence, and adult. During late fetal development, mammary epithelial ductal structures form a rudimentary ductal tree within the mesenchymal-derived mammary fat pad [3–5]. In prepubescent female mice, this rudimentary ductal tree remains mostly stagnant. However, in response to the systemic circulation of ovarian sex hormones starting at puberty (3–4 wk of age), active ductal progression begins [6] and continues until the female mouse reaches 10–12 wk of age, at which time the mammary fat pad is entirely infiltrated [4, 7]. The mammary tissue at late pubescence is often referred to as "resting". Here, we reveal how dynamic the "resting" mammary gland can be, and demonstrate the cellular basis for its changing morphology.

Tissue inhibitors of metalloproteinases (TIMPs) are a family of genes capable of inhibiting the activity of the matrix metalloproteinase (MMP) superfamily [8]. MMPs are broadly grouped into interstitial collagenases, stromelysins, gelatinases, elastase, and membrane-type enzymes, which collectively degrade the basement membrane matrix and stromal matrix [9]. The activity of these gene families is often up-regulated during physiological and pathological tissue turnover [8, 10]. To date, several studies have examined the relationship of these 2 gene families in breast cancer [11] and mammary development [7, 12, 13], but none have examined whether they are regulated during the estrous cycle in mammary glands. The fact that these genes are synchronized during ovarian and uterine remodeling [14, 15] and mammary involution [16] indicates that they may also be precisely expressed during mammary gland remodeling associated with the estrous cycle. In summary, our data provide insight into the influence of the estrous cycle, systemic sex hormones, and matrix regulatory genes on mammary gland biology.

## MATERIALS AND METHODS

### *Animals and Estrous Stage Determination*

Stages of estrous were determined by cytological evaluation of vaginal smears as described previously [17]. Mature virgin female C57/BL6 mice aged 12–14 wk were given vaginal smears twice daily and only those mice undergoing normal estrous cycle changes over at least 2 cycles were included in further studies. In this group, vaginal smears were taken twice daily (at 0900 h and again at 1200 h), and those exhibiting a stage change at noon were divided into diestrus, proestrus, or metestrus groups and were killed immediately. Thus, all samples collected are representative of the initial onset of each stage, and this regimen minimized the expected in-

[1]Supported by grant MT-13251 from the Medical Research Council of Canada. J.E.F. was supported by a University of Toronto Open Scholarship.
[2]Correspondence: Rama Khokha, Department of Medical Biophysics, Ontario Cancer Institute, 610 University Avenue, Toronto, ON, Canada M5G 2M9. FAX: 416 946 2984; e-mail: rkhokha@oci.utoronto.ca

Received: 28 November 2000.
First decision: 26 December 2000.
Accepted: 6 April 2001.

ISSN: 0006-3363. http://www.biolreprod.org

trastage variation. Because mice enter estrus in the early hours of the night, vaginal smears were obtained at 2100 and 0900 h, and those mice that entered estrus from proestrus overnight were killed immediately. All samples were coded for subsequent double blind analyses. Mice were cared for in accordance with regulation established by the Canadian Council for Animal Care under the protocols approved by the Animal Care Committee of the Ontario Cancer Institute, Toronto, Ontario.

### *Serum Levels of Progesterone and 17β-Estradiol*

Approximately 1 ml of blood was removed from each mouse when it was killed, placed at room temperature for 30 min, and then centrifuged at 6000 × *g* to isolate serum. Serum samples were stored at −70°C until processed for 17β-estradiol and progesterone by Dr. S. Tokmakejian (University of Western Ontario, Canada) using protocols that have been previously used for measurements of these hormones in mice [18]. Briefly, for progesterone and 17β-estradiol, 300 μl of serum was extracted and aliquots of the extract were evaporated and reconstituted in diluent 9 and in diluent 3 (both from Chiron Diagnostic, Walpole, MA), respectively. Progesterone was measured by a competitive chemiluminescent assay (ACS-180 analyzer; Chiron Diagnostic). 17β-Estradiol was measured by a competitive enzyme immunoassay on an Immuno-1 analyzer (Bayer Diagnostics, Berkeley, CA).

### *Morphological and Histological Analysis of Mammary Glands*

To examine morphology, mammary glands were isolated from 12- to 14-wk-old females, and carmine-alum whole-mount staining was performed. One 4th-inguinal mammary fat pad was removed and placed on a microscope slide at room temperature for several minutes to adhere to the glass. The tissue was then fixed in Clarke fluid (75% ethyl alcohol, 25% acetic anhydride) for 16 h. After 30 min in 70% ethyl alcohol, the tissue was stained in a carmine-alum mix (0.2% carmine, 0.5% aluminum potassium sulphate) for 16 h, followed by 4–6 h of destaining (2% HCl, 70% ethyl alcohol). After dehydration in ascending concentrations of ethanol, the tissue was cleared in toluene. To store whole mounts, slides were rehydrated from toluene in 100% ethanol for 5 min (2×), followed by 5 min in each of 70%, 50%, 30% ethanol and then water. The air-dried slides maintained ductal contrast and could be restained or rehydrated in water. For histological analysis, mammary glands were fixed for 24 h in 4% (w/v) buffered-formalin, processed for sectioning (5 μm), and stained in hematoxylin and eosin. Whole mount and histological images were digitized using Northern Eclipse Software (Empix Imaging Inc., Toronto, ON, Canada). Mammary gland morphology on 29 mice was graded from 0 to 3 by two independent investigators using coded slides. Grades were assessed in 5 fields distal to the lymph node, and assigned as described in *Results* and *Discussion.* To determine the extent of intramouse variation, whole mount and histological analyses was performed on all pairs of the mammary glands from one mouse. This was repeated at least three times each in mice representing the strains FVB, C57/BL6, and CD1. Thus, a total of nine mice were tested.

### *Proliferating Cell Nuclear Antigen Immunostaining*

All proliferating cell nuclear antigen (PCNA) immunostaining was performed on the 4th-inguinal mammary gland. One 4th-inguinal mammary fat pad was removed, fixed for 3 h at 4°C in 4% paraformaldehyde, and embedded in paraffin. Sections were dewaxed in two changes of xylene, rehydrated through an ethanol series, and placed into 3% hydrogen peroxide for 10 min to block endogenous peroxidase activity. For antigen retrieval, slides were rinsed in water and microwaved in 10 mM citrate buffer pH 6.0. Slides were then rinsed in PBS, incubated with anti-PCNA (1:1000 dilution; Novocastra Laboratories Ltd., New Castle, U.K.) antibody for 1 h in a humidified chamber at room temperature, and then washed in PBS. Bound antibody was detected using the Level 2 Ultra Streptavidin Detection System (Signet Laboratories Inc., Dedham, MA) and fresh AEC substrate (3-amino-9-ethylcarbazole; Sigma, St. Louis, MO) as described by the manufacturer (Signet). Tissue was counterstained in Mayers hematoxylin, rinsed in PBS, and mounted with Crystal Mount (Biomeda Corp., Foster City, CA). This procedure labels PCNA-positive cells as dark red nuclei.

### *In Situ DNA End-Labeling*

Immunohistological staining of apoptotic cells was performed using published protocols [19]. Briefly, formalin-fixed sections from the 4th-inguinal mammary fat pad were dewaxed in two changes of xylene, rehydrated through an ethanol series, and placed into 3% hydrogen peroxide for 10 min to block endogenous peroxidase activity. After rinsing in water for 5 min, slides were treated with 0.4% pepsin pH 5.2 at 42°C for 10 min, followed by rinsing in water for 5 min. Slides were equilibrated in buffer A (50 mM Tris-HCl, 5 mM $MgCl_2$, 10 mM β-mercaptoethanol, 0.005% BSA fraction V pH 7.5) for 5 min at room temperature. Klenow (1 U/ml; Sigma) and 2.5 μM each of dATP, dCTP, dGTP, and biotin-labeled-dUTP (Sigma) in buffer A were applied to the sections and incubated at 42°C for 1 h. Slides were rinsed in water and incorporated biotin-labeled-dUTP was detected using the Level 2 Ultra Streptavidin Detection System (Signet) and counterstained as described in the previous section. This procedure labels apoptotic cells as dark red nuclei.

### *Histomorphometry*

All morphometric analyses were performed on the 4th-inguinal mammary fat pad using double-coded slides from five mice in each stage. The PCNA and apoptotic indices were derived separately from different slides, and each parameter was individually assessed for ductal and alveolar epithelium. The number of positive epithelial cells was divided by the total number of epithelial cells to calculate the fraction of positive cells. For the above indices, an average of 250 nuclei were scored on one section. No significant intrasample variation in apoptosis or PCNA was evident when multiple sections, derived from one mouse mammary gland, were quantified.

### *RNA Slot-Blot Analysis*

Total RNA was extracted from one 3rd-thoracic mammary gland as described previously [20]. Five micrograms of total RNA were slot-blotted on a Minifold II slot-blot system (Schleicher and Schuell, Keene, NH), as described by the manufacturer and hybridized with murine [α-$^{32}$P]dCTP-labeled DNA probes specific for TIMP-1, -2, -3, and -4; MMP-2, -3, -7, -9, and -13; and 18S ribosomal RNA. Radiolabeled DNA probes were generated by random priming using the Prime-It Kit (Stratagene, La Jolla, CA). To confirm that RNA was undegraded, 2 μg of total RNA were resolved on a 1.1% agarose/5.5% formaldehyde gel, transferred to GeneScreen Plus (NEN Research Product Inc., Boston, MA), and hybridized with a murine α-$^{32}$P-labeled dCTP DNA probe specific for 18S rRNA. Membrane prehybridization, hybridizations, and washes were performed following published protocols [21]. Quantification of radioactive signals was performed using a PhosphorImager and Image Quant Software (Molecular Dynamics, Sunnyvale, CA). RNA was obtained from seven mice at each stage of estrous cycle. For sequential probing, the membrane was stripped in 1% SDS, 2 mM EDTA for 5 min at 80°C. Complete stripping of the probe was confirmed by autoradiography before subsequent reprobing.

### *Statistical Analysis*

All data sets, except the apoptotic index, were found to be normally distributed when tested by the Shapiro-Wilks test. Overall, the following statistical analyses were performed. First, to assess if differences in the proliferation index or mRNA levels were statistically significant, ANOVA was performed on each group. If the entire group was significant at $P < 0.05$, then pairwise comparisons were made using the Fisher least significant difference (LSD) test. Differences were considered significant if they were in a group that passed the ANOVA test and an LSD test. A Mann-Whitney test was performed on apoptosis index to determine if significant differences existed between diestrus and nondiestrus stages for ductal and alveolar indices. Third, to determine the correlation between various indices, independent of the estrous stage, regression analysis was performed on the entire group of mice within the study, and the coefficient of correlation ($r$) was calculated. Curvilinear regression was used for alveolar apoptosis because the data most likely reflect a biological system in which a plateau of cellular apoptosis is reached.

## RESULTS

### *Secondary Branching and Alveolar Development Exhibit Specific Variations in Adult Mammary Tissue*

Mammary whole mount staining allows a three-dimensional visualization of epithelial ductal and alveolar structures against a translucent fatty background and readily re-

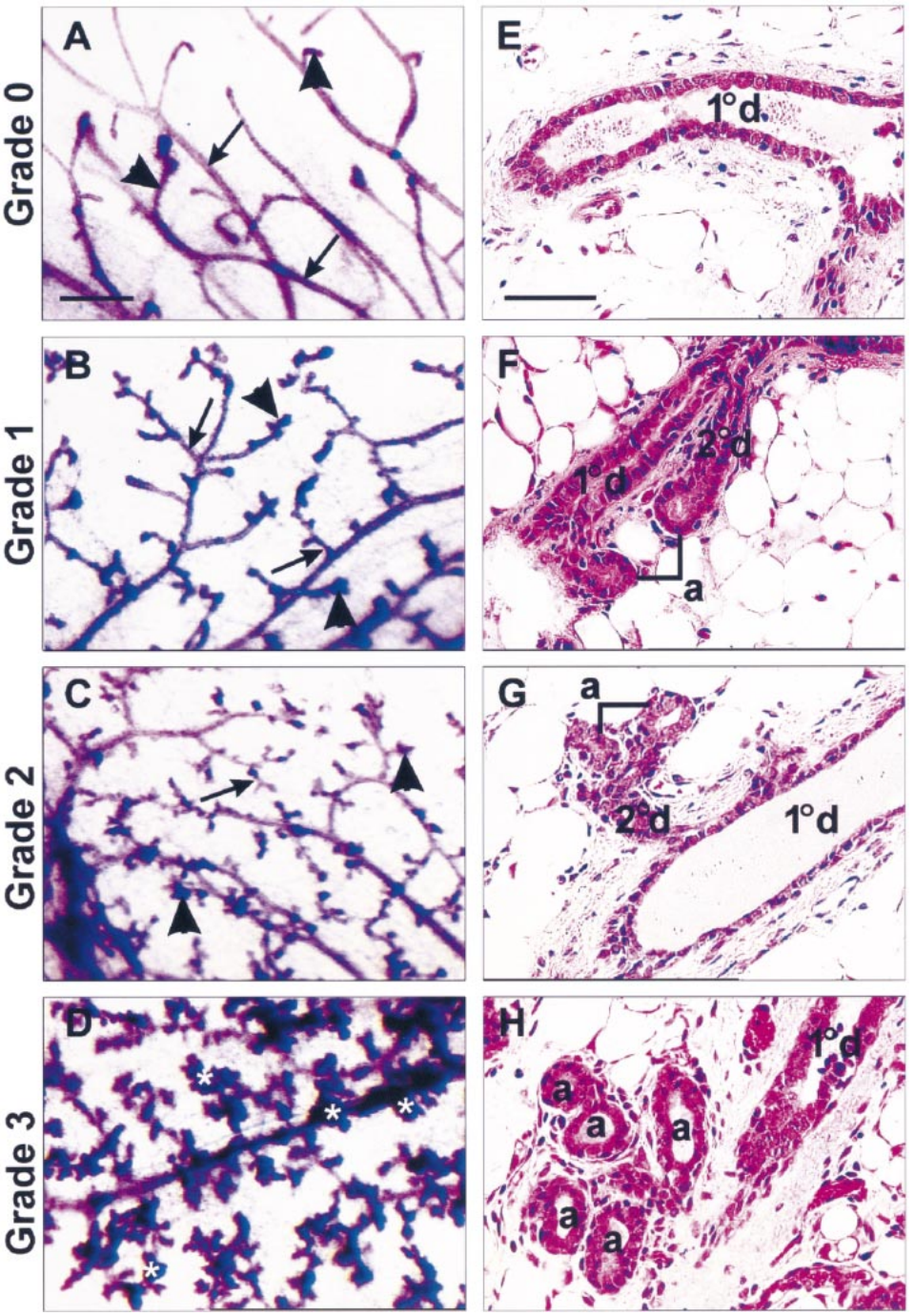


FIG. 1. Mammary morphology and histology exhibit specific variations in ductal and alveolar development in mouse. **A**–**D**) Whole mount and **E**–**H**) hematoxylin and eosin (H&E) staining of adult nulliparous mammary tissue. Grade 0 mammary morphology (**A**) displayed mostly primary ducts (arrows) and a limited number of secondary ducts (arrowheads). Grade 1 (**B**) exhibited increased secondary branching (arrows) and with emanating alveolar buds (arrowheads). Grade 2 (**C**) contained tertiary branches (arrow) and more alveolar buds (arrowheads), and grade 3 (**D**) showed full development of alveoli (asterisks). In the H&E sections, grade 0 (**E**) displayed mostly the primary ducts (1°d) and no alveoli. Grade 1 (**F**) contained secondary branching (2°d) and budding alveoli (a). Further development of alveolar structure (a) was evident in grade 2 (**G**). Fully developed alveoli (a) with extended lumens were found in grade 3 (**H**). Bars = 5 mm in **A**–**D**, and 50 μm in **E**–**H**.

veals the extent of ductal elongation, branching, and alveolar development. To uncover the extent of the normal physiological variation in mammary morphology, whole mount analysis was performed on mammary tissue taken from 29 adult nulliparous female mice. We visualized a spectrum of morphologies within the mammary tissue as illustrated in Figure 1, A–D. The morphological variations in mammary tissue stemmed from differences in secondary branching and alveolar development that we graded from 0 to 3. As shown in Figure 1, grade 0 tissue had limited secondary branches and a complete absence of alveolar structures (Fig. 1A); grade 1 tissue displayed one or two budding alveoli emanating from secondary ducts (Fig. 1B); grade 2 consisted of increased numbers of secondary ducts and higher order branching, both containing several budding alveoli structures (Fig. 1C); and grade 3 was similar to grade 2 in the extent of branching, but extensive numbers of fully developed alveoli emanated from secondary branches (Fig. 1D). Histological analysis of grade 0 revealed mostly primary ducts and the absence of alveolar budding (Fig. 1E). Grade 1 tissue exhibited initiation of alveolar buds from secondary branching (Fig. 1F), whereas grade 2 often revealed further alveolar growth (Fig. 1G). Grade 3 resembled lobulo-alveolar structures seen in mammary tissue during early gestation. Groups of alveoli were clearly evident throughout mammary tissue exhibiting grade 3 morphology (Fig. 1H). Lumen size of alveolar structures increased with grade, whereas ductal lumens showed no overt differences. We also observed similar mammary morphological variations in the other strains of

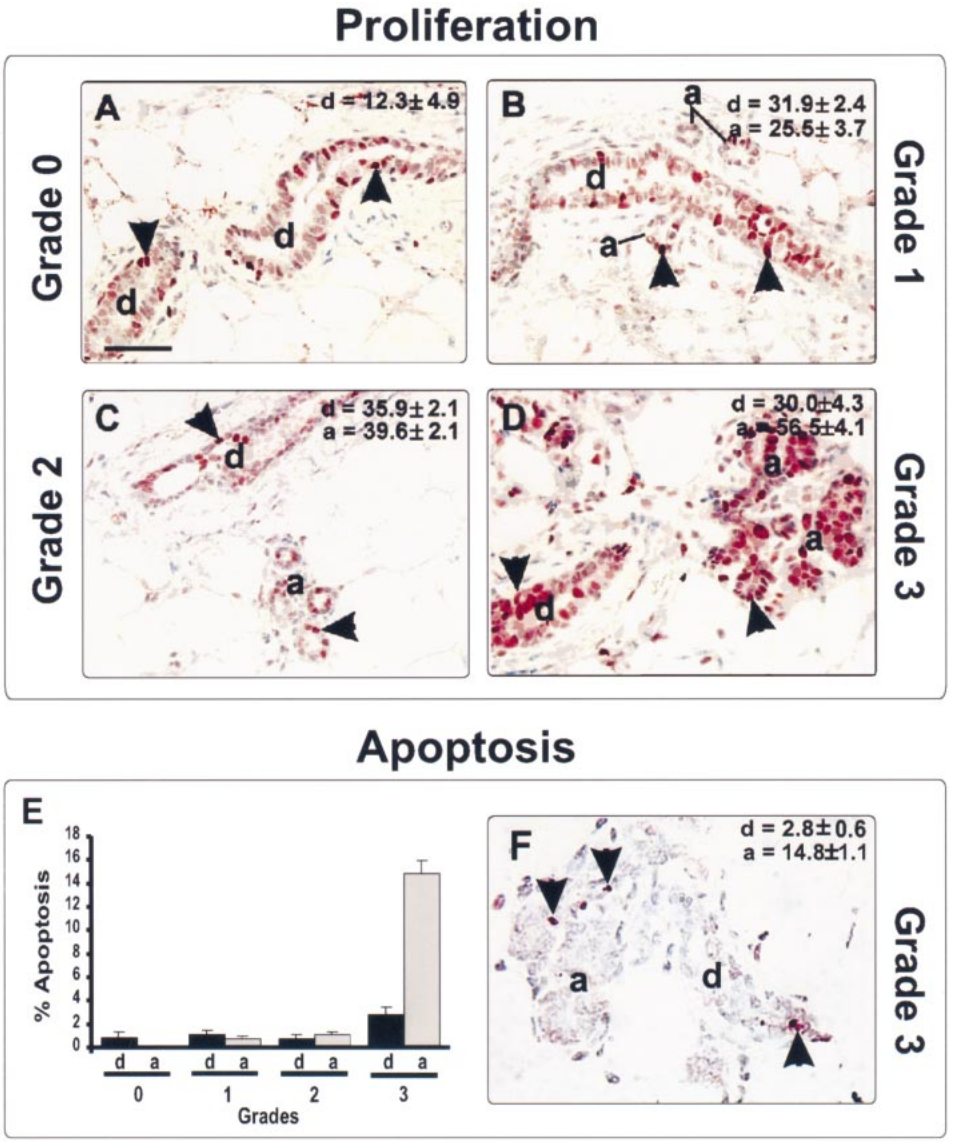


FIG. 2. Mammary ductal epithelium and alveolar epithelium differ in proliferation and apoptosis indices. **A**–**D**) PCNA immunostaining and **E**, **F**) in situ DNA end-labeling of mammary tissue exhibiting different morphological grades. Proliferation or apoptotic indices (mean ± SEM; top right of each panel) were derived from five mice in each group, and values were calculated separately for ductal (d) and alveolar (a) epithelium. PCNA-positive cells appeared dark red in their nuclei. Ducts (d) at all grades contained epithelium that was PCNA-immunopositive (**A**–**C**; arrowheads). Proliferation was much less in ductal epithelium found in grade 0 mammary tissue (**A**) compared with ductal epithelium in grades 1, 2, and 3 (**B**–**D**). The proliferation index for alveolar epithelium (a) significantly increased with each successive morphological grade from 1 to 3 (**B**–**D**). Quantification of apoptosis revealed that few apoptotic cells were found in ductal and alveolar epithelium of grades 0, 1, and 2 (**E**). However, the apoptotic index for alveolar epithelium in grade 3 was ~14-fold higher than all other grades (**E**). As shown in a representative section (**F**), many alveolar and some epithelial cells labeled positive for apoptosis in grade 3 morphology. Apoptotic nuclei are stained a dark red (arrowheads). Bar (**A**–**D** and **F**) = 50 μm.

mice, including the inbred FVB and the outbred CD1. These inherent variations in mammary morphology clearly demonstrate the gross differences that can exist within this organ. We observed no overt intramouse variation among the five pairs of mammary tissues (not shown). Moreover, ductal structure and alveolar development did not deviate within any single mammary gland (not shown). Therefore, the morphology of any one mammary gland was an appropriate representation of the morphology of other mammary glands within the same mouse.

### *Mammary Ductal Epithelium and Alveolar Epithelium Differ in Proliferation and Apoptotic Indices*

In order to explore the cellular processes that are responsible for the morphological changes noted above, we assessed mammary epithelial proliferation and apoptosis as a function of grade using immunohistochemistry. Figure 2 represents changing PCNA labeling, an indicator of DNA synthesis [22], in mammary epithelial cells in both ductal and alveolar structures. PCNA is a processivity factor for DNA polymerase and is often used as an indicator of DNA synthesis in mammary epithelial cells [7, 23, 24]. The number of PCNA-positive cells increased in ductal epithelium between grade 0 to grade 1 tissues (Fig. 2, A and B; $P < 0.05$). This induction of proliferation may reflect an initiation of sprouting of secondary ducts noted at grade 1. Ductal epithelial proliferation did not increase further as the branching morphology progressed to grade 3, suggesting that secondary branching is ongoing at these grades (Fig. 2, B–D). In contrast, the steady increase in alveolar proliferation that occurred with each increment of mammary grade from 1 to 3 was significant (Fig. 2, B–D; $P < 0.05$). This led to alveolar proliferation and ductal proliferation that differed significantly from each other within mammary tissue exhibiting grade 3 morphology (Fig. 2D; $P < 0.001$). The selective increase in alveolar proliferation explains the maturation of these structures seen at the whole mount level (Fig. 1, D and E). Ductal and alveolar apoptosis remained relatively low, and not significantly different, in mammary tissues of grades 0, 1, or 2 (Fig. 2E). In contrast, grade 3 morphology displayed extensive apoptosis in alveolar structures that was approximately 14-fold higher than at any other stage (Fig. 2, E and F). Ductal epithelial apoptosis in grade 3 mammary glands was also elevated in comparison to all other grades (Fig. 2, E and F). It is clear that grade 3 mammary morphology represents a unique window of

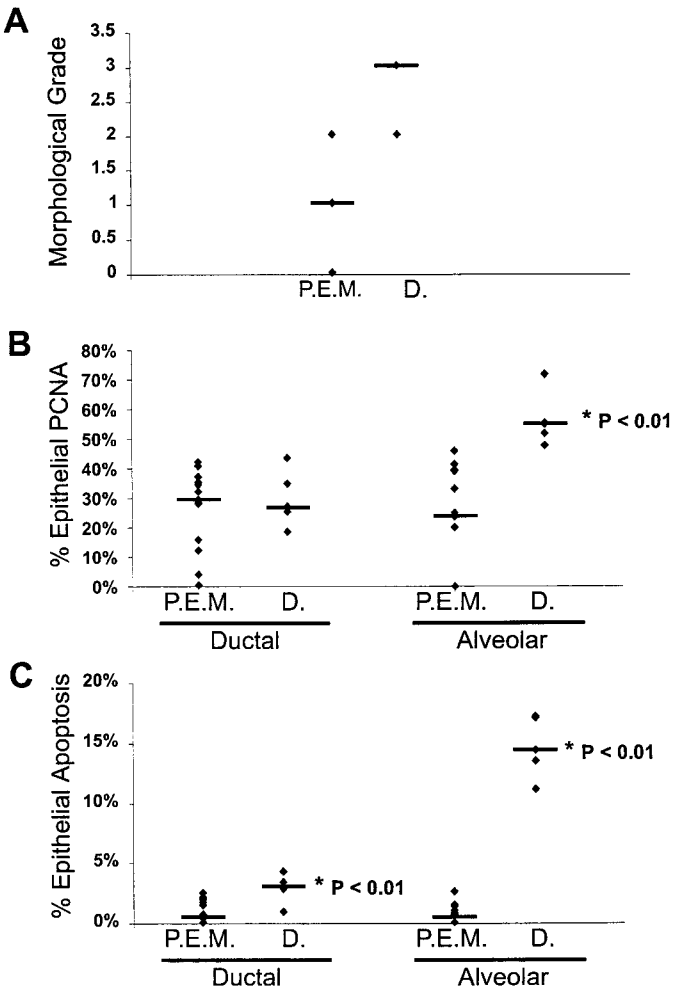


FIG. 3. Mammary grade, epithelial proliferation, and apoptosis are highest at diestrus. **A**) Quantitative comparison of mammary grade, **B**) PCNA labeling, and **C**) apoptosis in nondiestrus (proestrus, estrous, and metestrus) versus diestrus mammary glands. Nondiestrus stages (n = 21) had grades ranging from 0 to 2 but did not exhibit grade 3, whereas seven of eight mice at diestrus displayed grade 3, and the eighth mouse was grade 2 (**A**). No significant differences were evident in the percentage of PCNA-positive ductal epithelial cells between nondiestrus (n = 15) and diestrus stages (n = 5; **B**). A significant increase in alveolar epithelial proliferation occurred at diestrus versus nondiestrus (**B**). Both ductal and alveolar epithelial apoptosis were significantly greater in mammary glands at diestrus (n = 5) versus nondiestrus (n = 15; **C**). **A**–**C**) Are represented as a scatter plot with median indicated. Asterisks designate significant differences based on the Mann-Whitney test.

mammary gland development. It encompasses extensive proliferation and apoptosis simultaneously, with the majority of these cellular processes being inherent to alveolar epithelial cells, and not ductal.

### *Fully Developed Alveoli Are Seen Exclusively at Diestrus*

The female reproductive cycle produces cyclical variations in the levels of progesterone and 17β-estradiol that are driven by the ovary. The murine reproductive cycle (estrous cycle) spans 4–5 days compared with the human menstrual cycle of 28–30 days [25]. Our approach was to carefully stage (see experimental procedures) the estrous cycle status of each female mouse, but to perform subsequent morphological and cellular analysis without knowing the estrous stage from which the samples were taken. Upon decoding, we found that proestrus, estrous, and metestrus each exhibited mixed mammary morphologies of grades 0, 1, or 2. In contrast, grade 3 was exclusively seen at diestrus (Fig. 3A). Of the eight females classified as diestrus, seven exhibited grade 3 mammary morphology, whereas the 21 females from all other stages varied between grades 0 and 2. Diestrus was also the stage at which alveolar proliferation (Fig. 3B), ductal apoptosis (Fig. 3C), and alveolar apoptosis (Fig. 3C) were significantly greater than the combined averages of nondiestrus stages. Therefore, diestrus, which represents the end of the luteal phase, is unlike all other estrous cycle stages in that it represents the most differentiated mammary gland state.

TABLE 1. Serum levels of 17β-estradiol and progesterone as a function of the murine estrous cycle.

| Estrous stage | Estradiol* (pg/ml) | Progesterone* (ng/ml) |
|---|---|---|
| Proestrus | 47.3 ± 2.1 | 8.1 ± 1.8 |
| Estrus | 66.0 ± 3.2 | 1.2 ± 0.5 |
| Metestrus | 50.3 ± 3.2 | 7.7 ± 0.9 |
| Diestrus | 51.3 ± 3.2 | 18.4 ± 3.6 |

* Values are presented as mean ± SEM, n = 8 mice/estrous stage.

### *Natural Levels of Progesterone, and Not 17β-Estradiol, Correlated Positively with Mammary Epithelial Proliferation and Apoptosis*

We measured the nonmanipulated serum levels of the hormones progesterone and 17β-estradiol at a window that represents the initial onset of each estrous stage, which allowed us to assess mammary changes as a function of the physiological fluctuations of these hormones. We observed a 40% increase in the average serum concentration of 17β-estradiol from proestrus (47.3 ± 2.1 pg/ml) to estrus (66.0 ± 3.2 pg/ml) as shown in Table 1. As expected, 17β-estradiol levels declined after ovulation at metestrus. In contrast, the average progesterone levels (mean ± SEM in Table 1) decreased from proestrus (8.1 ± 1.8 ng/ml) to estrus (1.2 ± 0.5 ng/ml), and were maximal at diestrus (18.4 ± 3.6 ng/ml). Overall, a 15-fold decrease in progesterone levels was seen from diestrus to estrus. The substantial drop of progesterone at estrus is a function of regression of the corpora lutea (luteolysis) in mice, as it is in humans, when implantation does not occur. Our sample size established trends for each hormone that followed the known physiological changes in the murine ovary [17] and reflects serum levels that have been previously reported for these hormones in mouse [18]. It is important to note however, that our serum hormone levels represent the initial onset of each estrous stage and may not be representative of the later part of the stage. An in-depth analysis of the serum levels of progesterone and 17β-estradiol in the mouse has been established before, in which multiple time points throughout each estrous stage were examined [18].

In the present investigation, we found that progesterone levels correlated positively and significantly with morphological grade (Fig. 4A) and alveolar proliferation (Fig. 4B), but not ductal proliferation (Fig. 4C). We found it intriguing that progesterone levels also correlated positively with ductal apoptosis (Fig. 4E). Moreover, the relationship between progesterone and alveolar apoptosis exhibited a curvilinear relationship (Fig. 4D). This indicates that the apoptotic response by the majority of alveolar epithelial cells toward progesterone levels may occur only after a threshold level of ~12 ng/ml of progesterone is reached. In contrast to progesterone, circulating levels of 17β-estradiol did not

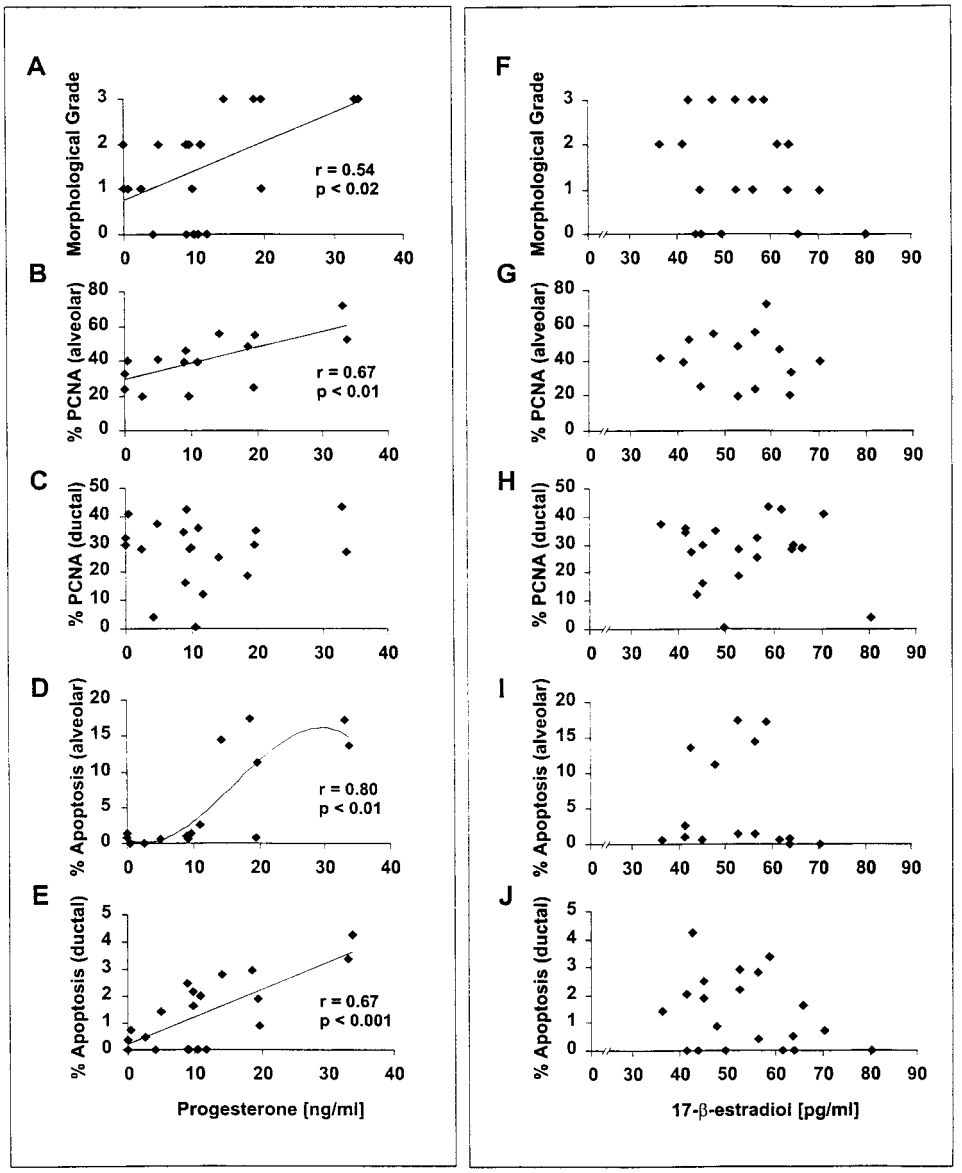


FIG. 4. Relationships between of systemic progesterone, 17β-estradiol levels, mammary morphology, cellular proliferation, and apoptosis. **A**) Mammary morphology, **B**) alveolar proliferation, and **E**) ductal apoptosis exhibited positive correlations with serum progesterone levels. **D**) The alveolar apoptotic index suggests that these cells have a curvilinear relationship with progesterone, with most apoptosis occurring when progesterone is >12 ng/ml. No relationship is evident between progesterone and ductal proliferation (**C**) or between 17β-estradiol and mammary morphology (**F**), cellular proliferation (**G** and **H**), and apoptosis (**I** and **J**). $r$ = correlation coefficient. Each data point represents one mouse.

correlate with mammary morphological grade (Fig. 4F), epithelial proliferation (Fig. 4, G and H), or epithelial apoptosis (Fig. 4, I and J).

### *Estrous Cycle-Mediated Tissue Turnover in Mammary Gland Entails Regulation of TIMPs and MMPs*

Slot-blot analysis revealed that specific TIMPs and MMPs were differentially regulated at the mRNA level in the mammary gland during the estrous cycle. All four TIMPs were expressed throughout the estrous cycle. TIMP-2, -3, and -4 had increased mRNA levels at proestrus and metestrus when compared with estrus and diestrus (Fig. 5, A and B; and data not shown). In contrast, TIMP-1 was constitutively expressed at low levels (not shown). The increases in the mRNA levels of TIMP-3 ($P < 0.02$) and TIMP-4 ($P < 0.01$) at proestrus and metestrus were significant. All MMPs that were examined (MMP-2, -3, -7, -9, and -13) were expressed in the mammary gland at each stage of the estrous cycle. However, only MMP-9 and MMP-13 displayed significant differential regulation at the mRNA level (Fig. 5, C and D). The increase in MMP-9 mRNA at metestrus was significant when compared with the increase at proestrus (Fig. 5C; $P < 0.01$). Significant changes were also found in MMP-13, which exhibited a greater than twofold increase in it's mRNA at proestrus and at metestrus, compared with the estrus and diestrus stages (Fig. 5D; $P < 0.0005$). It is intriguing that only TIMP-4 and MMP-13 exhibited strong associations with other mammary gland estrous cycle-associated characteristics. Specifically, TIMP-4 negatively correlated with both lobulo-alveolar grade ($r = -0.41$; $P < 0.05$) and epithelial proliferation ($r = -0.44$; $P < 0.01$), and MMP-13 negatively correlated with $E_2$ concentration ($r = -0.53$; $P < 0.005$). These data indicate that the estrous cycle influences the expression of specific TIMPs and MMPs in the mammary gland.

## DISCUSSION

Here we provide the first full characterization of nulliparous murine mammary glands during the estrous cycle. Specifically, morphological, cellular, and molecular changes were assessed, and their correlation with natural systemic levels of progesterone and 17β-estradiol were determined. Figure 6 is a schematic representation of our findings and

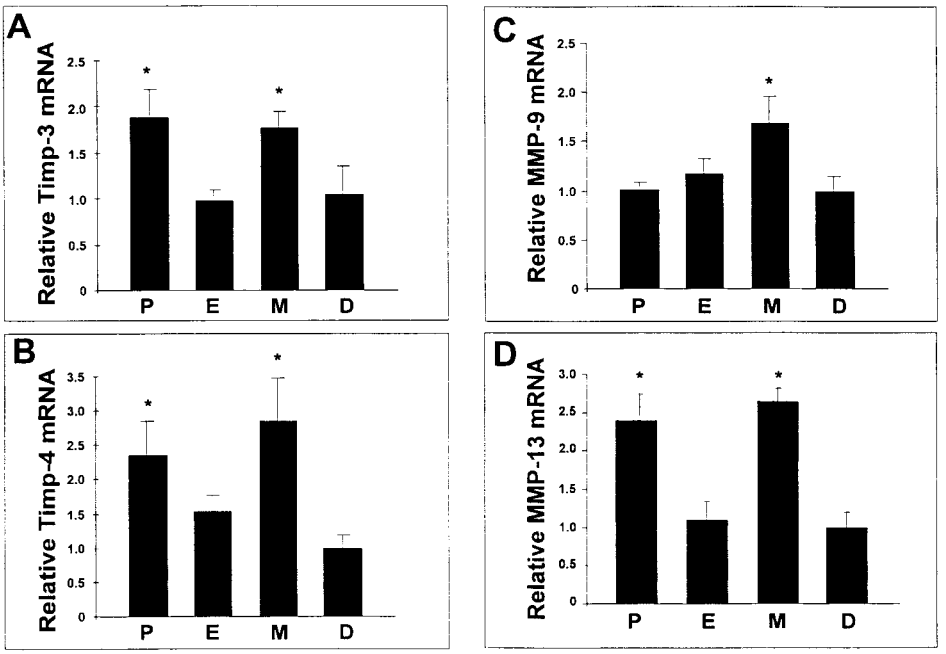


FIG. 5. Coregulation of mammary TIMPs and MMPs during the estrous cycle. Relative expression of TIMP-3 (**A**; $*P < 0.02$), TIMP-4 (**B**; $*P < 0.01$), MMP-9 (**C**; $*P < 0.01$), and MMP-13 (**D**; $*P < 0.0005$) mRNAs in mammary glands taken at proestrus (P), estrus (E), metestrus (M), and diestrus (D). Seven mice were analyzed at each stage of the estrous cycle. Following the quantification of the radioactive signal by the PhosphorImager analysis and Image Quant software, means and SEM were calculated for each estrous stage. For each probe, the lowest mean value was taken as 1, and fold differences were calculated. SEMs were adjusted by the same magnitude. All mRNA levels were normalized to 18S rRNA.

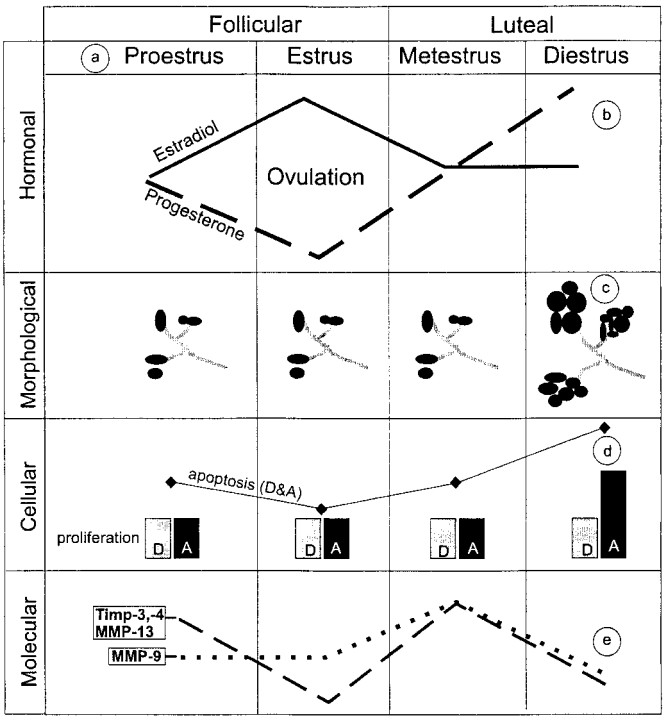


FIG. 6. Schematic representation of estrous cycle-dictated hormonal, morphological, cellular, and molecular changes in the mouse mammary gland. Proestrus, metestrus, and diestrus data were derived from samples collected at noon (within 3 h of entry into the stage), whereas estrus data were from samples obtained at 0900 h (within 12 h into the stage), as described in *Materials and Methods.* Maximum 17β-estradiol levels were observed at estrus, whereas progesterone levels were highest at diestrus (**b**). Diestrus was the stage when lobulo-alveolar structures were fully developed (**c**). Alveolar (A) proliferation/apoptosis and ductal (D) proliferation peaked at diestrus (**d**). Expression profiles of TIMP-3, TIMP-4, and MMP-13 mRNAs exhibit specific increases at proestrus and metestrus. MMP-9 mRNA levels were maximal at metestrus. The mRNAs of all TIMPs and MMPs examined were minimal at diestrus (**e**).

serves to illustrate the number of orchestrated changes in the mammary gland that occur during the estrous cycle.

The role of progesterone and estrogen in dictating murine mammary morphology has been studied following their exogenous administration or in estrogen and progesterone receptor knockout mice [26–29]. This work has implicated estrogen in stimulating ductal elongation, and progesterone in inducing ductal branching and lobulo-alveolar growth. Our results further support the role of progesterone in eliciting alveolar growth during the estrous cycle, because we found strong association between the natural levels of this hormone and alveolar proliferation, but not ductal proliferation. Progesterone receptor-positive as well as progesterone receptor-negative ductal epithelial cells have been found adjacent to each other [30] and evidence suggests that ductal epithelium contains cell lineages for both ducts and alveoli [31]. Our findings, which examined the mammary gland in response to systemic progesterone, suggest the existence of two distinct mammary epithelial cell populations, one (ductal) nonresponsive, and the other (alveolar) responsive to rising progesterone levels associated with the estrous cycle.

Cole et al. [32] was the first to identify morphological differences in the mouse mammary gland associated with the estrous cycle. However, these measurements were from young (6-wk-old) female mice, and included ductal diameter changes and terminal end bud differences, and not alveolar growth or regression. Analysis of rat mammary gland morphology during the estrous cycle indicates that alveolar growth is greatest at estrus, although the extent of this growth is marginal [33]. Therefore, differences between mouse and rat mammary glands in response to hormones appear to be species-dependent. Our findings on mammary epithelial proliferation but not apoptosis differ from that of Andres et al. [34]. In a hunt for novel protein tyrosine kinases, these authors found that DNA synthesis in the mouse mammary gland is greatest during late proestrus and estrus [34]. However, their measurements did not differentiate between alveolar epithelium and ductal epithelium, and were not from a defined window within each estrous stage. In addition, their data were obtained from

analyzing thymidine incorporation in short-term mammary gland cultures. Because we measured these indices in vivo, and at early but not late proestrus, it is difficult to directly compare their findings with ours. Within the murine uterus, two peaks of luminal epithelial proliferation are known to occur during the estrous cycle, one at proestrus and the other at late metestrus [18]. However, our data are more similar to those found in the human female breast, in which epithelial proliferation is highest during the late luteal phase [35], and in hamsters in which the mitotic index was greatest during diestrus [36].

Of interest, is the curvilinear relationship between progesterone and alveolar apoptosis. Because the majority of alveolar cells exhibited a greater than 10% apoptotic rate when progesterone was >12 ng/ml, and little apoptosis was seen in these cells bathed in <12 ng/ml, we propose that alveolar regression occurs only after a certain threshold of progesterone is reached. However, very high progesterone levels are reached during pregnancy without the onset of alveolar apoptosis occurring, which suggests that other factors must be considered in this hypothesis. Possibly, prosurvival signals during pregnancy override the apoptotic response toward high serum levels of progesterone. In support of this, progesterone alone, at a concentration equivalent to the third trimester of human pregnancy, has been shown to be proapoptotic for the breast cancer cell line, T47-D [37]. However, further compounding the story is the finding that the local release of progesterone into postlactational involuting mammary tissue inhibits epithelial apoptosis [38]. It is obvious that the murine estrous cycle, pregnancy, and postlactational involution are physiologically distinct and we suggest that the mammary epithelial apoptotic response to progesterone depends on all the intricacies of the extracellular environment (hormonal, structural, and mechanical), and therefore, mammary epithelial apoptosis is likely dependent on more than changes in progesterone level alone. The overlap of proliferation and apoptosis that we observed in the mouse at diestrus is temporally similar to that in human breast tissue. In humans, the peaks of proliferation and apoptosis are only 3 days apart within the luteal phase, with proliferation occurring first [35]. Within the murine estrous cycle, diestrus is a prolonged stage in comparison to the other stages, as it can last up to 2.5 days before proestrus initiates [39]. We suggest that this extended time is necessary for the depletion of alveoli (by apoptosis) that form at the beginning of diestrus.

Although we found no significant correlations with 17β-estradiol and mammary epithelial proliferation or apoptosis, the importance of this hormone in mammary physiology cannot be understated. Several groups have suggested that 17β-estradiol acts on estrogen receptor-positive mesenchymal breast tissue and stimulates production of growth factors that in turn influence the parenchyma [40]. It has also been proposed that the action of 17β-estradiol is mediated through the up-regulation of prolactin or mammary epithelium progesterone receptors [40]. In the latter case, progesterone may mediate its effects following the estrogen priming of the mammary tissue. Studies examining the mammary epithelial mitotic response to administered 17β-estradiol, progesterone, or both, have revealed that both can induce DNA synthesis within 24 h [26, 41]. Therefore, because of this lag time in response, our measure of proliferation may also reflect an earlier event (approximately one stage earlier) of initiation into the cell cycle.

During the mouse estrous cycle, the majority of tissue turnover occurred in alveolar structures and this dedifferentiation is similar in character and magnitude to that seen in postlactational mammary involution in which lobulo-alveoli undergo extensive apoptosis in response to the hormonal, structural, and mechanical signals [16, 38, 42, 43]. During lactation, functional lobulo-alveoli are surrounded by an intact basement membrane, which is degraded in part by MMPs during their postlactational involution [13]. We believe that similar events are occurring during the estrous cycle in mice, but in a much shorter time span. The significant increase in MMP-9 and MMP-13 mRNAs at proestrus and metestrus, and their temporal coregulation with TIMP-3 and TIMP-4 mRNAs suggested that basement membrane and interstitial matrix remodeling are precisely controlled during the murine estrous cycle. We have previously reported an up-regulation of TIMP mRNAs (TIMP-1 and TIMP-3) at proestrus in the murine ovary [17]. Moreover, the inherent tissue turnover associated with female reproductive tissues in response to changing hormones often involves coregulation of TIMPs and MMPs [14].

Mammary transgenic mice or knockouts of proto-oncogenes, tumor suppressors, growth factors, and cell-surface receptors have been examined for the proliferative/apoptotic response of mammary epithelial cells to these molecules [44–52]. One question is whether it is important to map the estrous stage while determining mammary phenotypes in nulliparous female mice. Because most phenotypes are initially determined at the morphological level, it will be important to account for the natural variation described in this report. At the cellular level, the analysis of mammary epithelial proliferation, apoptotic indices, or both in experimental animals would require estrous staging as these indices correlated with progesterone levels. Based on our findings we further suggest that mammary epithelial proliferation, apoptosis, or both should be specified independently for ducts and alveoli, given the large differences between the two structures.

## ACKNOWLEDGMENTS

We thank J. Ho, P. Waterhouse, M.L. Weir, O. Sanchez-Sweatman, and K. Gowing for scientific discussions and technical help; and Dr. S. Minken for guidance with statistical analysis.

## REFERENCES

1. Rosen JM, Humphreys R, Krnacik S, Juo P, Raught B. The regulation of mammary gland development by hormones, growth factors, and oncogenes. Prog Clin Biol Res 1994; 387:95–111.
2. Vonderhaar BK. Regulation of development of the normal mammary gland by hormones and growth factors. Cancer Treat Res 1988; 40: 251–266.
3. Hovey RC, McFadden TB, Akers RM. Regulation of mammary gland growth and morphogenesis by the mammary fat pad: a species comparison. J Mammary Gland Biol Neoplasia 1999; 4:53–68.
4. Robinson GW, Hennighausen L, Johnson PF. Side-branching in the mammary gland: the progesterone-Wnt connection. Genes Dev 2000; 14:889–894.
5. Kratochwil K. Tissue combination and organ culture studies in the development of the embryonic mammary gland. Dev Biol 1985; 4: 315–333.
6. Daniel CW, Silberstein GB. Postnatal development of the rodent mammary gland. In: Neville MC, Daniel CW (eds.), The Mammary Gland: Development, Regulation, and Function. New York: Plenum Press; 1987: 3–31.
7. Fata JE, Leco KJ, Moorehead RA, Martin DC, Khokha R. TIMP-1 is important for epithelial proliferation and branching morphogenesis during mouse mammary development. Dev Biol 1999; 211:238–254.
8. Gomez DE, Alonso DF, Yoshiji H, Thorgeirsson UP. Tissue inhibitors

of metalloproteinases: structure, regulation and biological functions. Eur J Cell Biol 1997; 74:111–122.
9. Nagase H, Woessner JF Jr. Matrix metalloproteinases. J Biol Chem 1999; 274:21491–21494.
10. Shapiro SD. Matrix metalloproteinase degradation of extracellular matrix: biological consequences. Curr Opin Cell Biol 1998; 10:602–608.
11. Benaud C, Dickson RB, Thompson EW. Roles of the matrix metalloproteinases in mammary gland development and cancer. Breast Cancer Res Treat 1998; 50:97–116.
12. Witty JP, Wright JH, Matrisian LM. Matrix metalloproteinases are expressed during ductal and alveolar mammary morphogenesis, and misregulation of stromelysin-1 in transgenic mice induces unscheduled alveolar development. Mol Biol Cell 1995; 6:1287–1303.
13. Werb Z, Ashkenas J, MacAuley A, Wiesen JF. Extracellular matrix remodeling as a regulator of stromal-epithelial interactions during mammary gland development, involution and carcinogenesis. Braz J Med Biol Res 1996; 29:1087–1097.
14. Fata JE, Ho A, Leco KJ, Moorehead RA, Khokha R. Cellular turnover and extracellular matrix remodeling in female reproductive tissues: functions of metalloproteinases and their inhibitors. Cell Moll Life Sci 2000; 57:77–95.
15. Hulboy DL, Rudolph LA, Matrisian LM. Matrix metalloproteinases as mediators of reproductive function. Mol Hum Reprod 1997; 3:27–45.
16. Talhouk RS, Bissell MJ, Werb Z. Coordinated expression of extracellular matrix-degrading proteinases and their inhibitors regulates mammary epithelial function during involution. J Cell Biol 1992; 118: 1271–1282.
17. Inderdeo DS, Edwards DR, Han VK, Khokha R. Temporal and spatial expression of tissue inhibitors of metalloproteinases during the natural ovulatory cycle of the mouse. Biol Reprod 1996; 55:498–508.
18. Walmer DK, Wrona MA, Hughes CL, Nelson KG. Lactoferrin expression in the mouse reproductive tract during the natural estrous cycle: correlation with circulating estradiol and progesterone. Endocrinology 1992; 131:1458–1466.
19. Wijsman JH, Jonker RR, Keijzer R, van de Velde CJ, Cornelisse CJ, van Dierendonck JH. A new method to detect apoptosis in paraffin sections: in situ end-labeling of fragmented DNA. J Histochem Cytochem 1993; 41:7–12.
20. Chomczynski P, Sacchi N. Single-step method of RNA isolation by acid guanidinium thiocyanate-phenol-chloroform extraction. Anal Biochem 1987; 162:156–159.
21. Church GM, Gilbert W. Genomic sequencing. Proc Natl Acad Sci U S A 1984; 81:1991–1995.
22. Kelman Z. PCNA: structure, functions and interactions. Oncogene 1997; 14:629–640.
23. Fata JE, Kong YY, Li J, Sasaki T, Sasaki JI, Moorehead RA, Elliott R, Scully S, Voura EB, Lacey DL, Boyle WJ, Khokha R, Penninger JM. The osteoclast differentiation factor osteoprotegerin-ligand is essential for mammary gland development. Cell 2000; 103:41–50.
24. Lundgren K, Montes de Oca Luna R, McNeill YB, Emerick EP, Spencer B, Barfield CR, Lozano G, Rosenberg MP, Finlay CA. Targeted expression of MDM2 uncouples S phase from mitosis and inhibits mammary gland development independent of p53. Genes Dev 1997; 11:714–725.
25. Chabbert-Buffet N, Djakoure C, Maitre SC, Bouchard P. Regulation of the human menstrual cycle. Front Neuroendocrinol 1998; 19:151–186.
26. Bresciani T. Effect of ovarian hormones on the duration of DNA synthesis in cells of the C3H mouse mammary gland. Exp Cell Res 1965; 38:13–32.
27. Daniel CW, Silberstein GB, Strickland P. Direct action of 17 beta-estradiol on mouse mammary ducts analyzed by sustained release implants and steroid autoradiography. Cancer Res 1987; 47:6052–6057.
28. Lydon JP, DeMayo FJ, Funk CR, Mani SK, Hughes AR, Montgomery CA Jr, Shyamala G, Conneely OM, O'Malley BW. Mice lacking progesterone receptor exhibit pleiotropic reproductive abnormalities. Genes Dev 1995; 9:2266–2278.
29. Couse JF, Korach KS. Estrogen receptor null mice: what have we learned and where will they lead us? Endocr Rev 1999; 20:358–417.
30. Silberstein GB, Van Horn K, Shyamala G, Daniel CW. Progesterone receptors in the mouse mammary duct: distribution and developmental regulation. Cell Growth Differ 1996; 7:945–952.
31. Smith GH. Experimental mammary epithelial morphogenesis in an in vivo model: evidence for distinct cellular progenitors of the ductal and lobular phenotype. Breast Cancer Res Treat 1996; 39:21–31.
32. Cole HA. The mammary gland of the mouse, during the oestrus cycle, pregnancy and lactation. Proc R Soc Lond B Biol Sci 1933; 114:136–161.
33. Lotz W, Krause R. Correlation between the effects of neuroleptic on prolactin release, mammary stimulation and the vaginal cycle in rat. J Endocrinol 1978; 76:507–515.
34. Andres AC, Strange R. Apoptosis in the estrous and menstrual cycles. J Mammary Gland Biol Neoplasia 1999; 4:221–228.
35. Anderson TJ, Ferguson DJ, Raab GM. Cell turnover in the ''resting'' human breast: influence of parity, contraceptive pill, age and laterality. Br J Cancer 1982; 46:376–382.
36. Purnell DM, Saggers GC. Topologic assessment by use of whole mounts of mitotic activity in the hamster mammary gland during the estrous cycle. J Natl Cancer Inst 1974; 53:825–828.
37. Formby B, Wiley TS. Progesterone inhibits growth and induces apoptosis in breast cancer cells: inverse effects on Bcl-2 and p53. Ann Clin Lab Sci 1998; 28:360–369.
38. Feng Z, Marti A, Jehn B, Altermatt HJ, Chicaiza G, Jaggi R. Glucocorticoid and progesterone inhibit involution and programmed cell death in the mouse mammary gland. J Cell Biol 1995; 131:1095–1103.
39. Laguchev SS. Comparison of the estrous cycles in mice of high and low cancer lines. Bull Eksp Biol Med 1962; 53:318–321.
40. Haslam SZ. Role of sex steroid hormones in normal mammary gland function. In: Niskanen E, Daniel CW (eds.), The Mammary Gland: Development, Regulation, and Function. New York: Plenum Press; 1987: 499–510.
41. Shyamala G. Roles of estrogen and progesterone in normal mammary gland development. Trends Endocrinol Metab 1997; 8:34–39.
42. Rosfjord EC, Dickson RB. Growth factors, apoptosis, and survival of mammary epithelial cells. J Mammary Gland Biol Neoplasia 1999; 4: 229–237.
43. Uria JA, Werb Z. Matrix metalloproteinases and their expression in mammary gland. Cell Res 1998; 8:187–194.
44. Vilotte JL, Huillier P, Mercier JC. Modification and repression of genes expressed in the mammary gland using gene targeting and other technologies. J Mammary Gland Biol Neoplasia 1998; 3:351–362.
45. Dickson C, Creer A, Fantl V. Mammary gland oncogenes as indicators of pathways important in mammary gland development. Oncogene 2000; 19:1097–1101.
46. Dankort DL, Muller WJ. Signal transduction in mammary tumorigenesis: a transgenic perspective. Oncogene 2000; 19:1038–1044.
47. Stepanova L, Finegold M, DeMayo F, Schmidt EV, Harper JW. The oncoprotein kinase chaperone CDC37 functions as an oncogene in mice and collaborates with both c-myc and cyclin D1 in transformation of multiple tissues [In Process Citation]. Mol Cell Biol 2000; 20: 4462–4473.
48. Tekmal RR, Kirma N, Gill K, Fowler K. Aromatase overexpression and breast hyperplasia, an in vivo model—continued overexpression of aromatase is sufficient to maintain hyperplasia without circulating estrogens, and aromatase inhibitors abrogate these preneoplastic changes in mammary glands. Endocr Relat Cancer 1999; 6:307–314.
49. Jamerson MH, Johnson MD, Dickson RB. Dual regulation of proliferation and apoptosis: c-myc in bitransgenic murine mammary tumor models. Oncogene 2000; 19:1065–1071.
50. Li M, Lewis B, Capuco AV, Laucirica R, Furth PA. WAP-TAg transgenic mice and the study of dysregulated cell survival, proliferation, and mutation during breast carcinogenesis. Oncogene 2000; 19:1010–1019.
51. Liao DJ, Natarajan G, Deming SL, Jamerson MH, Johnson M, Chepko G, Dickson RB. Cell cycle basis for the onset and progression of c-Myc-induced, TGFalpha-enhanced mouse mammary gland carcinogenesis. Oncogene 2000; 19:1307–1317.
52. Delmas V, Pla P, Feracci H, Thiery JP, Kemler R, Larue L. Expression of the cytoplasmic domain of E-cadherin induces precocious mammary epithelial alveolar formation and affects cell polarity and cell-matrix integrity. Dev Biol 1999; 216:491–506.